ISSN 0967-859X
THE SOCIETY FOR EARTHQUAKE AND CIVIL ENGINEERING DYNAMICS

NEWSLETTER

Volume 23 No 3
March 2012

SBFEM Special Issue

In this issue

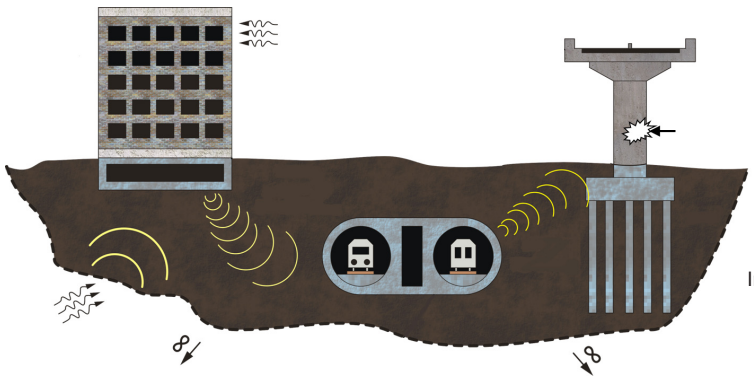

Image courtesy of B. Radmanović (Sofistik AG)

Editorial introduction

We are delighted to present in this issue of the Newsletter an article by Bojan Radmanović and Casimir Katz about a novel computational procedure with wide applications. This procedure, named the Scaled Boundary Finite Element Method (SBFEM), is interesting – not least because it is directly applicable to problems which so far the Finite Element Method (FEM) or the Boundary Element Method (BEM) have struggled to solve in an entirely satisfactory way.

However, it is unreasonable to assume that all readers of the Newsletter are acquainted with the SBFEM. Therefore, the following short introduction serves to provide an overview of the history and the salient features of the method. The introduction is based almost entirely on the monograph published in 2003 by J.P. Wolf (Ref. 1) and does not take into account more recent developments. The origins of the SBFEM can be traced back to the 70's. As with many other breakthroughs in science and engineering, it appears that researchers worked on similar theories at the same time without knowing about each other's work. In the early 90's two of the key figures – Choming Song and John P. Wolf – embarked on a fruitful collaboration which lead to the publication of several articles and eventually in 1996 a book (Ref. 2). By this time the method was known as the Consistent Infinitesimal Finite Element Cell Method, but soon after the more succinct "SBFEM" was coined. In the subsequent decade further progress was made in placing the method on a more solid theoretical foundation, and numerous papers appeared on the topic. Today, Google Scholar returns 555 results for "SBFEM" – a number which

nevertheless is still dwarfed by searches for "BEM" (91,600) or "FEM" (742,000).

The SBFEM is similar to the BEM in so far as only the surface of the body under consideration needs to be meshed. The interior of the body is not discretised. As a consequence, the SBFEM results in a system with fewer unknowns (degrees-of-freedom) than the FEM which requires a mesh encompassing the entire volume of the body. However, the SBFEM avoids the limitations and theoretical complexity of the BEM, whilst offering the same flexibility and versatility as the FEM (with some important exceptions as noted below).

The efficiency of the SBFEM relies on the following approach. The behaviour of a solid body is governed by partial differential equations (PDEs) which must be satisfied throughout the domain of the body. In its attempt to solve these PDEs, the SBFEM introduces a new curvilinear coordinate system with one radial and two circumferential directions. The circumferential directions are everywhere tangential to the surface of the body. The PDEs are transformed into this coordinate system. The boundary of the object is then divided into surface elements with simple shape functions mapping the response in the two circumferential directions. These surface elements are equivalent to standard finite elements, and their mathematical representation is obtained by finite element techniques (e.g. the method of weighted residuals). This reduces the governing equations to a set of ordinary differential equations in the radial coordinate, which can be solved analytically and without loss of accuracy.

An important feature, which the SBFEM shares with the BEM, is the ability to model unbounded domains with little extra effort. Unbounded domains is one area which does not suit the FEM. As described in, for instance, Ref. 3, the FEM toolbox currently has a number of competing techniques for modelling unbounded domains, but none of these has so far proved to be exact or satisfactory in all circumstances. Another notable advantage of the SBFEM is found in the method's ability to account for discontinuities and stress concentrations with relative ease and great accuracy.

However, the SBFEM also has its limitations, and at least three are immediately discernible. Firstly, it is clear that the SBFEM cannot compete with the FEM in modelling civil engineering structures that render themselves to beam and shell idealisations. Secondly, it appears that highly heterogeneous solids with step changes in properties such as layered geological sites would be difficult to model. And thirdly, it seems that nonlinear behaviour – such as that manifested in material plasticity or large displacement effects – is still beyond the reach of the SBFEM.

For the practising civil engineer or analyst, the most promising application probably lies in joint application of the FEM and the SBFEM – much in the same way as the FEM previously has been used with the BEM. For example, it may be envisaged that in problems involving static and dynamic soil-structure interaction, the near-field (i.e. the region of interest) can be modelled by finite elements, while the far-field can be modelled by scaled boundary finite elements. This combination allows the use of (nonlinear) beam and shell elements for the structure, and (nonlinear) solid brick elements for the near-field soil. The dynamic stiffness required at the boundary of near-field region is provided with great accuracy by the SBFEM.

Thus, the SBFEM is ideally suited for the substructure method in structural dynamics. The assumption of a rigid basemat is not required. The Winkler foundation, which has been used in the past for flexible basemats although it is not suitable for dynamic analysis, could be made redundant by the SBFEM. In the direct method, scaled boundary finite elements could replace the viscous boundary proposed some 40 years ago by Lysmer and Kuhlemeyer, although this application undoubtedly would increase the computational cost.

In conclusion, it would be great news if in the not too distant future engineers and analysts had access to the SBFEM as another tool in prominent FE packages. It is hoped that the following article will create some preliminary awareness of this interesting development.

References

[1] Wolf JP, *The Scaled Boundary Finite Element Method*, John Wiley & Sons, 2003

[2] Wolf JP & Song Ch, *Finite Element Modelling of Unbounded Media*, John Wiley & Sons, 1996

[3] Nielsen AH, Boundary conditions for seismic analysis, S*ECED Newsletter,* **21**(3), 2009

SECED

SECED, The Society for Earthquake and Civil Engineering Dynamics, is the UK national section of the International and European Associations for Earthquake Engineering and is an affiliated society of the Institution of Civil Engineers. It is sponsored by the Institution of Mechanical Engineers, the Institution of Structural Engineers, and the Geological Society. The Society is also closely associated with the UK Earthquake Engineering Field Investigation Team. The objective of the Society is to promote co-operation in the advancement of knowledge in the fields of earthquake engineering and civil engineering dynamics including blast, impact and other vibration problems. For further information about SECED contact: The Secretary, SECED, Institution of Civil Engineers, One Great George Street, London, SW1P 3AA, UK. Or visit the SECED website: http://www.seced.org.uk

Dynamic Soil-Structure Interaction Using an Efficient Scaled Boundary Finite Element Method in Time Domain with Examples

Bojan Radmanović
Sofistik AG
bojan.radmanovic@sofistik.de

Casimir Katz
Sofistik AG
casimir.katz@sofistik.de

Abstract

In this paper a substructure method is used for the solution of the dynamic soil-structure interaction problem in which the soil is modelled using a scaled boundary finite element method (SBFEM) in time domain, while the structure is modelled using a finite element method. A governing equation of the SBFEM, in which the unknown is a fully populated acceleration unit-impulse response matrix, requires solution of the matrix integral equation involving convolution integrals. In this paper we use a new procedure developed by authors in their previous work, which brings two essential improvements to the original method: (1) A new scheme, which assumes piece-wise linear change of the acceleration unit-impulse response matrix, is used and in combination with an extrapolation parameter and linearization for the late times provides more robustness and efficiency to the solution. For the examples analysed by authors no instabilities where present for a wide range of parameters. (2) The soil-structure interaction vector described by the convolution integral is evaluated using a new and efficient recursive scheme based on integration by parts. These two enhancements lead to a very significant reduction of computation effort and a linear dependency with time. Using the new method a two- and three-dimensional benchmark and practical examples of the dynamic wave-soil-structure interaction are analysed. The results are compared with more conventional procedures for the modelling of the unbounded soil like the lumped-parameter or the boundary element method. The examples show the accuracy and high computational efficiency of the proposed discretization schemes and qualify the new approach for the usage in large practical problems encountered in vibration and earthquake engineering.

1 Introduction

Dynamic soil-structure interaction is an important phenomenon which in general cannot be ignored when performing dynamic analysis of structures founded on soft soil. Apart from the positive role that the soil can play in the overall dynamic behaviour of the soil-structure system, it can also have negative influence on the structural performance [1]. The true nature of the behaviour of the soil-structure system subjected to dynamic excitation is a complex matter, often leading to non-intuitive results, which only emphasizes the importance of the proper study of this matter.

In this paper dynamic soil-structure interaction is modelled using a substructure method [2][3][4]. The structure (together with a part of the adjacent soil) is modelled by a standard finite-element method while the unbounded soil is modelled using the scaled boundary finite elements (Figure 1). The connection between the two substructures is assured by the interaction vector $\mathbf{r}_b(t)$ acting at the soil-structure interface, which can be described by the convolution integral

$$\mathbf{r}_b(t) = \int_0^t \mathbf{M}_b^{\infty}(t)[\ddot{\mathbf{u}}_b^t(t-\tau) - \ddot{\mathbf{u}}_b^g(t-\tau)]d\tau \qquad (1)$$

where $\mathbf{M}_b^{\infty}(t)$ represents the acceleration unit-impulse

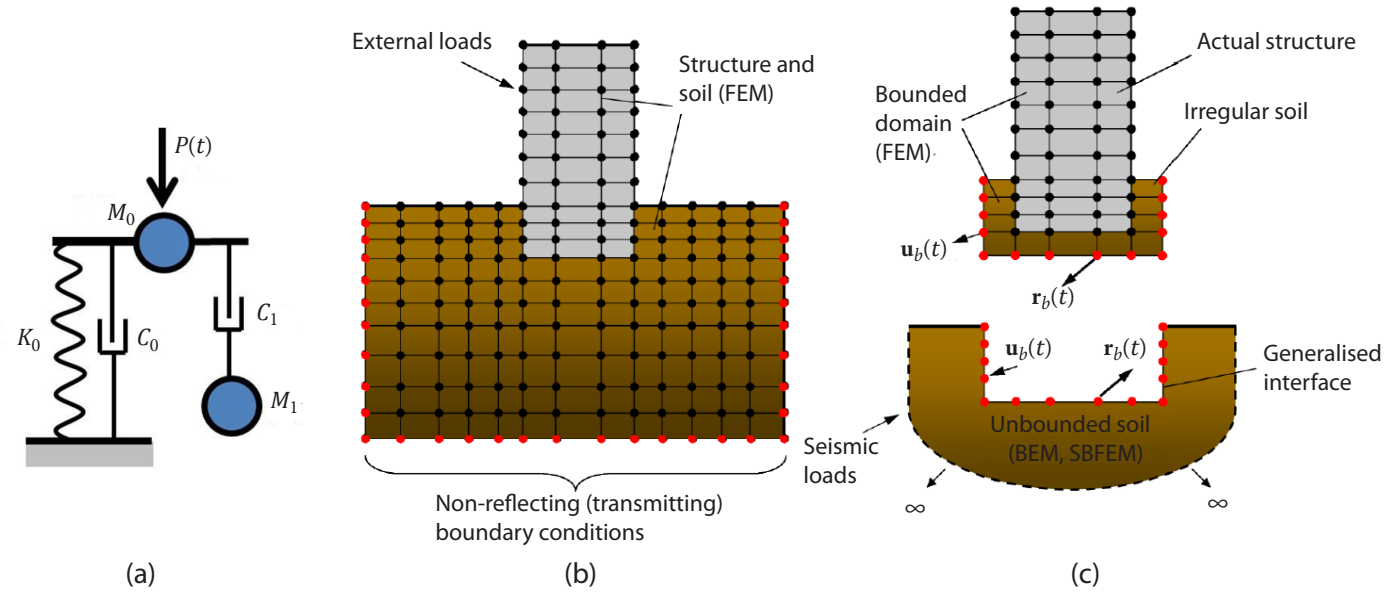

Figure 1. Methods to model SSI: (a) Lumped-parameter (b) Direct (c) Substructure method.

response matrix and $\ddot{\mathbf{u}}(t)$ is the acceleration vector. Subscript b denotes the nodes at the soil-structure interface, belonging to both the structure and the soil. Superscript t indicates that the motion of the structure is referred to an origin that does not move (total motion). The vector $\ddot{\mathbf{u}}_b^g(t)$ represents the so-called effective seismic foundation input motion. The superscript g denotes the system ground, i.e. the soil with excavation (scattered motion of the soil). The ground acceleration vector $\ddot{\mathbf{u}}_b^g(t)$ can be computed from the free-field motion of the soil (i.e. soil without excavation) [2][3] and it will be regarded as known.

The equations of motion of the structure can be expressed as

$$\begin{bmatrix}\mathbf{M}_{ss} & \mathbf{M}_{sb}\\ \mathbf{M}_{bs} & \mathbf{M}_{bb}\end{bmatrix}\begin{Bmatrix}\ddot{\mathbf{u}}_s^t\\ \ddot{\mathbf{u}}_b^t\end{Bmatrix}+\begin{bmatrix}\mathbf{C}_{ss} & \mathbf{C}_{sb}\\ \mathbf{C}_{bs} & \mathbf{C}_{bb}\end{bmatrix}\begin{Bmatrix}\dot{\mathbf{u}}_s^t\\ \dot{\mathbf{u}}_b^t\end{Bmatrix}+\begin{bmatrix}\mathbf{K}_{ss} & \mathbf{K}_{sb}\\ \mathbf{K}_{bs} & \mathbf{K}_{bb}\end{bmatrix}\begin{Bmatrix}\mathbf{u}_s^t\\ \mathbf{u}_b^t\end{Bmatrix}=\begin{Bmatrix}\mathbf{p}_s(t)\\ \mathbf{p}_b(t)\end{Bmatrix}-\begin{Bmatrix}\mathbf{0}\\ \mathbf{r}_b(t)\end{Bmatrix} \tag{2}$$

where $\mathbf{K}$, $\mathbf{C}$ and $\mathbf{M}$ are the stiffness, damping and mass matrices of structure, $\mathbf{u}(t)$, $\dot{\mathbf{u}}(t)$ and $\ddot{\mathbf{u}}(t)$ are the displacement, velocity and acceleration vectors, while $\mathbf{p}(t)$ is a force vector acting directly on the structure. Subscript s describes the nodes belonging only to the structure. To solve Equation 2 at time t vector $\mathbf{r}_b(t)$ must be known, which in turn means that the acceleration unit-impulse matrix $\mathbf{M}_b^{\infty}(t)$ must be known.

In this paper the acceleration unit-impulse response matrix is computed using the scaled boundary finite-element method (SBFEM) in time domain, developed by Wolf and Song [5][6]. This method was extended to modelling the non-homogeneous half-space by Bazyar and Song [7][8], where the non-homogeneity was described by material properties varying as a power function of Cartesian coordinates. The governing equation of the SBFEM in time domain is given as

$$\int_0^t \mathbf{m}_b^{\infty}(t-\tau)\mathbf{m}_b^{\infty}(\tau)d\tau+\alpha_1 t\int_0^t \mathbf{m}_b^{\infty}(\tau)d\tau+\mathbf{e}^1\int_0^t\int_0^{\tau}\mathbf{m}_b^{\infty}(\bar{\tau})d\bar{\tau}\,d\tau$$
$$+\int_0^t\int_0^{\tau}\mathbf{m}_b^{\infty}(\bar{\tau})d\bar{\tau}\,d\tau\,(\mathbf{e}^1)^T-t^3\mathbf{e}^2\,\mathrm{H}(t)/6-t\mathbf{m}^0\,\mathrm{H}(t)=\mathbf{0} \tag{3}$$

where $\mathbf{m}_b^{\infty}(t)$ represents the acceleration unit-impulse response matrix in transformed coordinates, $\mathbf{e}^1$, $\mathbf{e}^2$ and $\mathbf{m}^0$ are transformed SBFE matrices, α_1 is a parameter of non-homogeneity and $\mathrm{H}(t)$ is a Heaviside function [7][8]. This integral equation has no analytical solution and in order to be solved, discretization in time must be applied. The original integration scheme for the solution of Equation 3 described in [5][6][7][8] assumes a piece-wise constant approximation of the acceleration unit-impulse response matrix within a time step, and it is only conditionally stable with a small critical step size. At each time station the convolution integrals in Equations 2 and 3 must be evaluated, and a Lyapunov matrix equation in $\mathbf{m}_b^{\infty}(t)$ must be solved. Since the SBFEM is a global procedure, $\mathbf{M}_b^{\infty}(t)$ is a fully populated matrix. Also, the finite element mesh of the soil-structure interface must be fine enough to capture the main characteristics of the wave propagation. All these things combined lead to an enormous computation and memory effort for large systems.

In this paper we outline a new procedure developed by the authors in their previous work [9][10], which brings

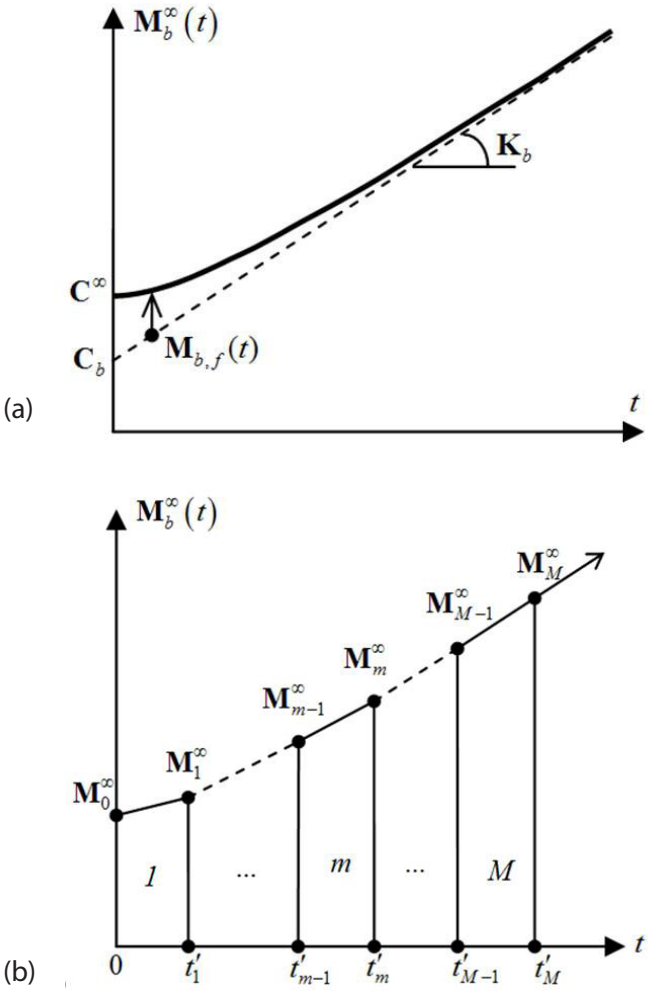

Figure 2. (a) Decomposition and (b) Linear discretization of $\mathbf{M}_b^\infty(t)$.

two essential improvements to the original integration schemes for the solution of the acceleration unit-impulse response matrix $\mathbf{M}_b^\infty(t)$ and the evaluation of the soil-structure interaction vector $\mathbf{r}_b(t)$. In order to increase the robustness and efficiency of the SBFEM, first the discretization scheme which assumes piece-wise linear change of $\mathbf{M}_b^\infty(t)$ in combination with an extrapolation parameter θ intended to provide more stability is used. To further increase the computation efficiency, a truncation time, after which $\mathbf{M}_b^\infty(t)$ is linearized, is introduced. Then, a new and very efficient scheme based on integration by parts is used for the evaluation of the soil-structure interaction vector. In the second part of this paper we apply the new method to two- and three-dimensional examples of the dynamic soil-structure interaction.

2 New procedure

The acceleration unit-impulse response matrix has a nice property – for late times it converges towards a linear asymptote (Figure 2a). In other words it can be decomposed into three parts – a constant part $\mathbf{C}_b\mathrm{H}(t)$, a linear part $\mathbf{K}_b t\mathrm{H}(t)$ and a part which converges to zero as time approaches infinity $\mathbf{M}_{b,f}(t\to\infty)=0$ [5]:

$$\mathbf{M}_b^\infty(t)=\mathbf{C}_b\,\mathrm{H}(t)+\mathbf{K}_b t\,\mathrm{H}(t)+\mathbf{M}_{b,f}(t) \tag{4}$$

Here an interaction vector $\mathbf{r}_b(t)$ is computed at times $t_n=n\Delta t$, while the acceleration unit-impulse response matrix $\mathbf{M}_b^\infty(t)$ is computed at times $t'_m=m\Delta t'$, where $m\in[1,M]$ and $\Delta t'=N\Delta t$ (Figure 2b). After time $t'_M=t_{MN}=MN\Delta t$ linearization is applied, and $\mathbf{M}_b^\infty(t)$ is approximated with only one linear segment using extrapolation from the last time segment $[t'_{(M-1)}, t'_M]$. Therefore, the time interval $[0, t_n]$ is divided into m intervals with size $\Delta t'$ and $K=n-mN$ intervals with size Δt.

At $t=0$ the acceleration impulse-response matrix $\mathbf{M}_b^\infty(t)$ is equal to the dashpot matrix $\mathbf{C}^\infty$ which can be determined from the high frequency expansion of the dynamic stiffness matrix [5][6].

2.1 Integration of the SBFEM equation in time domain

The starting point for the derivation of the new integration scheme for Equation 3 is to assume that the transformed acceleration unit-impulse response matrix $\mathbf{m}_b^\infty(t)$ is piece-wise constant within each time step. Equation 3 is first solved for $\overline{\mathbf{m}}_b^\infty(\bar{t}_m)=\overline{\mathbf{m}}_{b,m}^\infty$ at the time $t_m=t'_{(m-1)}+\Delta t=t'_{(m-1)}+\theta\Delta t'$. The extrapolation parameter $\theta\geq 1$ is introduced to provide more stability. After $\overline{\mathbf{m}}_{b,m}^\infty$ is computed, $\mathbf{m}_b^\infty(t'_m)=\mathbf{m}_{b,m}^\infty$ is determined as follows (subscript b is dropped):

$$\mathbf{m}_m^\infty=(\theta-1)\theta^{-1}\mathbf{m}_{m-1}^\infty+\theta^{-1}\overline{\mathbf{m}}_m^\infty \tag{5}$$

As already mentioned, a truncation time t'_M is used, after which $\mathbf{m}_m^\infty$ is linearized. Numerical approximation of the evaluation of $\mathbf{m}_m^\infty$ for $\theta\in[1,2]$ is given by the following schemes depending on the current time interval m:

1. For the interval $m\in[1,2]$ the scheme becomes an algebraic Riccati matrix equation

$$\overline{\mathbf{m}}_m^\infty\mathbf{A}_m\overline{\mathbf{m}}_m^\infty+\mathbf{B}_m\overline{\mathbf{m}}_m^\infty+\overline{\mathbf{m}}_m^\infty\mathbf{B}_m^T+\mathbf{C}_m=\mathbf{0} \tag{6}$$

   where the coefficient matrices $\mathbf{A}_m$, $\mathbf{B}_m$ and $\mathbf{C}_m$ depend on θ.

2. For the interval $m\in[3,M]$ the scheme reduces to Lyapunov matrix equation

$$a_m\overline{\mathbf{m}}_m^\infty+\mathbf{B}_m\overline{\mathbf{m}}_m^\infty+\overline{\mathbf{m}}_m^\infty\mathbf{B}_m^T+\mathbf{C}_m=\mathbf{0} \tag{7}$$

   where similarly a_m and $\mathbf{B}_m$ depend on θ, while $\mathbf{C}_m$ contains integration of the convolution term

$$\mathbf{C}_m=\theta\sum_{j=3}^{m-1}conv_j+\overline{\mathbf{C}}_m \tag{8}$$

As a direct consequence of the linearization after time t'_M,

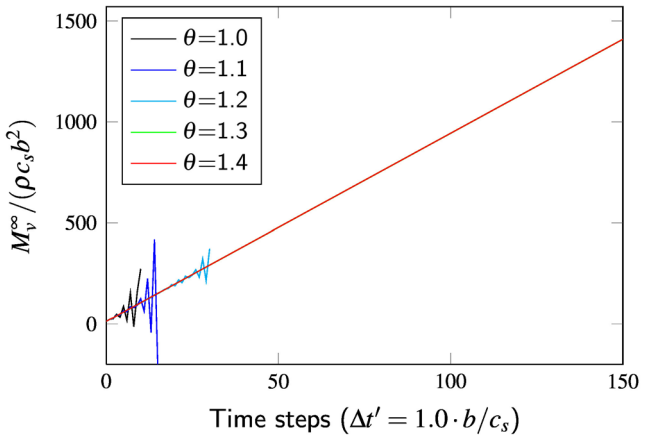

Figure 3. Effect of the extrapolation parameter on the stability of the new integration scheme for $\mathbf{M}_b^\infty(t)$. The original constant scheme is unstable for $\Delta t' \geq 0.125 b/c_s$.

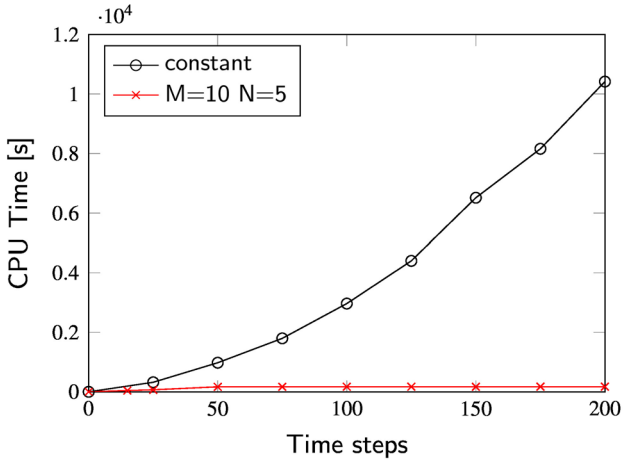

Figure 4. Comparison of CPU times required for the calculation of the response of the massless rigid foundation described in Subsection 2.3 for original (*const*) and new integration schemes.

the computation of acceleration unit-impulse response matrix $\mathbf{M}_b^\infty(t)$ is performed only up to the truncation time. Linearization of $\mathbf{M}_b^\infty(t)$ is previously exploited by Zhang et al [11], Yan et al [12] and Lehman [13][14]. Zhang et al [11] have based their procedure on the fact that the original discretization scheme with piece-wise constant approximation of $\mathbf{M}_b^\infty(t)$, although unstable for larger time steps, will produce satisfactory results for at least first 5 or 6 time intervals $\Delta t'$. With the piece-wise linear approximation and the introduction of extrapolation parameter θ, which provides more stability, the scheme proposed in [9] provides a more robust approach where a larger number of time steps can be used for the computation of $\mathbf{M}_b^\infty(t)$, before the truncation time is employed.

Figure 3 depicts the effect of the extrapolation parameter θ on the stability of the new scheme for the computation of $\mathbf{M}_b^\infty(t)$ for the prismatic rigid foundation described in Subsection 2.3. The original constant scheme is unstable for a time step $\Delta t'$ larger than $0.125 b/c_s$. The new linear scheme with θ = 1.0 has an even smaller critical time step size. But as we increase the extrapolation parameter θ, the stability increases, and with θ ≥ 1.3 no more oscillations persist for the observed time history. In all the examples analysed by authors no instabilities where present with θ ≥ 1.4.

2.2 Integration of the soil-structure interaction vector

The soil-structure interaction vector $\mathbf{r}_b(t)$ can be described by the convolution integral of the acceleration unit-impulse response matrix $\mathbf{M}_b^\infty(t)$ and the acceleration vector $\ddot{\mathbf{u}}_b(t)$:

$$\mathbf{r}_b(t) = \int_0^t \mathbf{M}_b^\infty(t)\left[\ddot{\mathbf{u}}_b^t(t-\tau) - \ddot{\mathbf{u}}_b^g(t-\tau)\right]d\tau \qquad (9)$$

To derive the new scheme for the evaluation of the soil-structure interaction vector, we start from the integration by parts of the functions $f(t)$ and $g(t)$, where $f(t)$ is linear in the interval $[t_1, t_2]$ while $g(t)$ is two times differentiable on the same interval:

$$\int_{t_1}^{t_2} f(\tau)\ddot{g}(t-\tau)d\tau = -f(t_2)\dot{g}(t-t_2) + f(t_1)\dot{g}(t-t_1) - \frac{[f(t_2)-f(t_1)][g(t-t_2)-g(t-t_1)]}{t_2-t_1} \qquad (10)$$

It is important to notice that the result of the integration in Equation 10 depends solely on the values at the end of the interval $[t_1, t_2]$, and that the function $g(t)$ can be an arbitrary two times differentiable function in this interval.

If instead of $f(t)$ and $g(t)$ we take $\mathbf{M}_b^\infty(t)$ and $\mathbf{r}_b(t)$ and if we assume the Newmark β-scheme for the integration of displacements, we can derive a new integration scheme for the evaluation of the soil-structure interaction vector as follows (subscript b is dropped where there is no possibility for confusion)

$$\mathbf{r}_b(t_n) = \mathbf{r}_{b,n} = [(a_1 - a_{10})\mathbf{M}_0^\infty + a_{10}\mathbf{M}_1^\infty]\mathbf{u}_n^t + \mathbf{q}_n \qquad (11)$$

where $a_1 = \gamma/(\beta\Delta t)$ and $a_{10} = 1/(N\Delta t)$, with β and γ representing the parameters of the Newmark scheme, and $\mathbf{u}_n = \mathbf{u}(t_n) = \mathbf{u}(n\Delta t)$ is the displacement vector. The vector $\mathbf{q}_n$ depends on the values $\mathbf{u}^t(t \leq t_{n-1})$ and $\ddot{\mathbf{u}}^g(t \leq t_n)$, which are known at time t_n, and it is given by the general formula

$$\mathbf{q}_n = \sum_{i=1}^{m} conv_i + \overline{\mathbf{q}}_n \qquad (12)$$

where *conv* is a convolution term. It should be noted that the convolution is only computed at the time stations $i = 1, M$. The original discretization scheme [6][8] requires n matrix-vector multiplications and $2n$ vector summations at each time step. The number of operations for the evaluation of Equation 11 involves $2M+5$ matrix-vector multiplications, 2 matrix and $6(M+1)$ vector summations. Since in practical applications $M << n$, the proposed scheme is very efficient.

Figure 4 shows the combined efficiency of the new compared to the original procedure from [6][8]. As can be seen from the figure, an originally quadratic dependency of CPU time with respect to the number of time steps is reduced to a linear dependency after the truncation time $t_{MN} = MN\Delta t$.

2.3 Accuracy and efficiency of the new procedure

To show the accuracy and efficiency of the new procedure, a three-dimensional example of a prismatic foundation embedded in an elastic homogeneous isotropic half-space is subjected to vertical triangular impulse point load with an amplitude P_0 and analysed (Figure 5).

The base of the foundation is square with length $2b$ and embedment depth $e = 2/3b$. The half-space is modelled without material damping and has shear modulus G, mass density ρ, shear wave velocity $c_s = \sqrt{(G/\rho)}$ and Poisson's ratio $\upsilon = 0.3$. The foundation-soil interface is modelled with 192 four-node quadrilateral scaled boundary finite elements.

The acceleration unit-impulse response matrix is calculated first using the original discretization scheme [5][7] (const) and then using the new procedure [9] described in Subsection 2.1. The extrapolation parameter is taken as $\theta = 1.4$. The time step size for the computation of the displacements is taken as $\Delta t = 0.05b/c_s$, while the time step size for the derivation of $\mathbf{M}_b^{\infty}(t)$ is $\Delta t' = N\Delta t$, where $N = \{2,3,5\}$. The truncation time, after which $\mathbf{M}_b^{\infty}(t)$ is linearized, is $t'_M = M\Delta t'$. At the end of the calculation, a rigid interface condition is enforced to make the results comparable. As can be seen from Figure 6, even for a very crude case of $M = 10$ and $N = 5$ there is an excellent agreement with the results obtained from the original constant integration scheme.

Figure 7 shows a time history of the vertical displacement of the foundation. Again excellent agreement is achieved.

Figure 8 shows the CPU time spent for the computation of the displacement response as a percentage of the CPU time need for the computation of the response using constant scheme. In the new procedure the majority of the CPU time is spent on the evaluation of the acceleration unit-impulse response matrix, but for larger systems and longer time histories, the evaluation of the soil-structure interaction vector plays a larger role in the total CPU time.

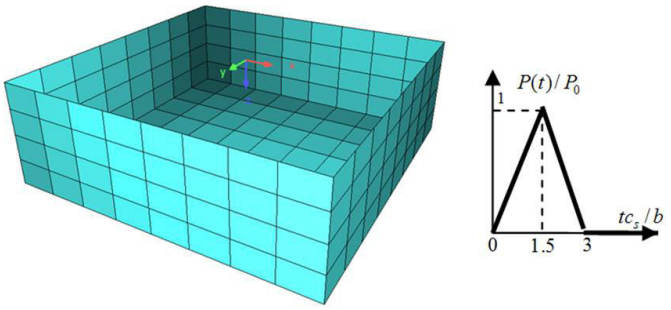

Figure 5. SBFE mesh of rigid massless prismatic foundation embedded in the half-space.

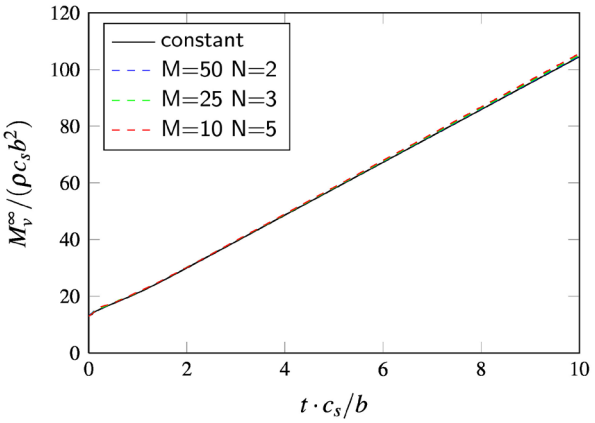

Figure 6. Vertical acceleration unit-impulse response coefficient of the rigid massless prismatic foundation. A rigid interface condition is enforced at the end of the calculation.

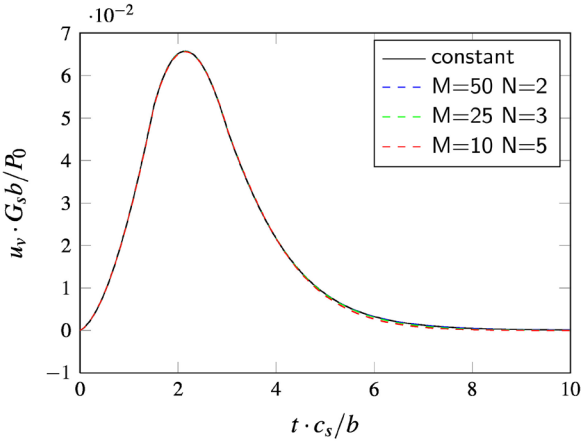

Figure 7. Vertical displacement response of the rigid massless prismatic foundation.

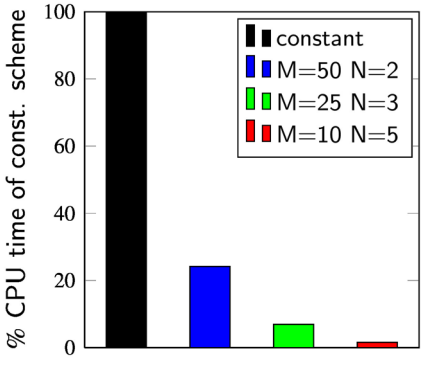

Figure 8. CPU time required for the computation.

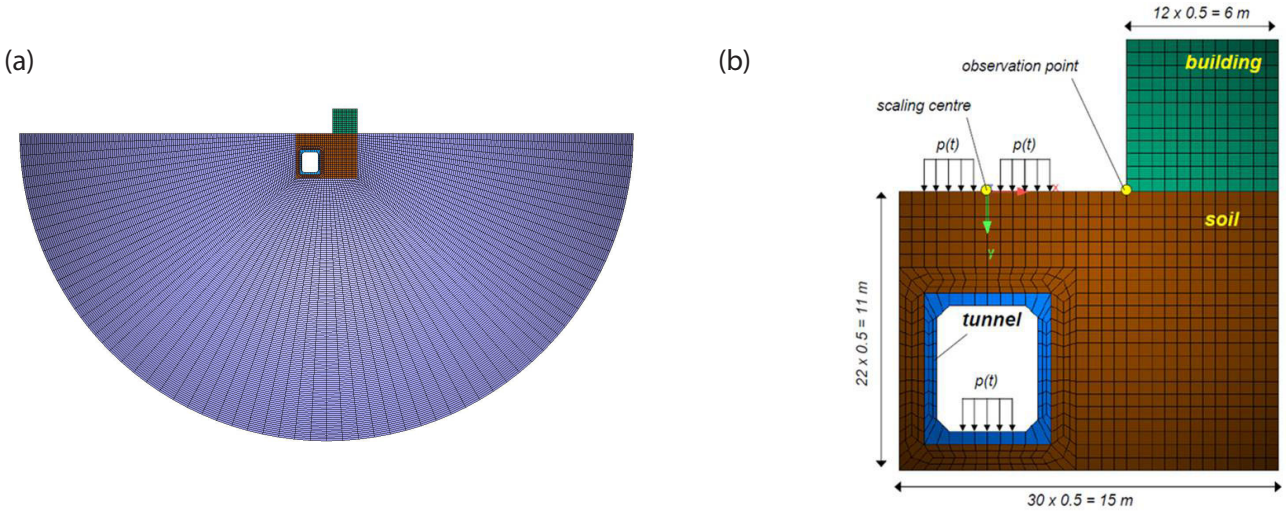

Figure 9. Road-tunnel traffic system: (a) EMM (b) Coupled SBFE/FE mesh.

3 Numerical examples

3.1 Road-tunnel traffic system

This two-dimensional plane strain road-traffic system based on the example previously analysed in [15] and [14] is intended to test the propagation of waves in a more complex environment. The results obtained using three methods to model unbounded soil – boundary element method (BEM), extended mesh method (EMM) and scaled boundary finite element method (SBFEM) – are compared.

The outline of the system is shown in Figure 9. The building has a square shape, dimensions 6×6m, with Young's modulus E = 3GPa, Poisson's ratio ν = 0.30 and mass density ρ = 2.0t/m^3. The tunnel has a rectangular shape, dimensions 5×6m, and is made of concrete with material properties E = 30GPa, ν = 0.33 and ρ = 2.0t/m^3. The near field of the soil also has a rectangular shape, dimensions 11×15m. The soil is homogeneous, elastic and isotropic with material properties E = 266MPa, ν = 0.33, ρ = 2.0t/m^3 and shear and dilatational soil wave velocities c_s = 224m/s and c_p = 386m/s. The structures and the soil are all modelled without material damping.

Boundary element method results (BEM) are taken from [15] and [14].

Extended mesh method (EMM) is based on a modelling of the large portion of the soil domain, so that the waves reflected from the artificially introduced boundary do not return back during the simulation time. For this example, this boundary is set at the distance $4b_s$ = 60m, where b_s = 15m represents the larger dimension of the near-field of the soil (Figure 9a).

For the SBFE method (Figure 9b), the structures (building and tunnel) and the soil near-field are modelled with the four-node quadrilateral finite elements, dimensions 0.5×0.5m, while the far-field is modelled with the two-node line scaled boundary finite elements which are applied at the interface between near- and far-field of the unbounded soil. The scaling point O is chosen to be at the centre of the coordinate system.

The system has been analysed under the Heaviside step line load $p(t)$ with amplitude of 1kN/m for $t \le 0.02$s, and 0 for $t > 0.02$s. The vertical displacement response of the observation point is recorded for the total time history equal to $t_{\max} = 640\Delta t$ (n = 640), where $\Delta t = 2.5\times10^{-4}$s. Before applying linearization, 20 (M = 20) acceleration unit-impulse response matrices $\mathbf{M}_b^{\infty}(t)$ with the time step size $\Delta t' = 5\Delta t$ (N = 5) are computed. Extrapolation parameter θ is set to 2.4.

Figure 10 shows the vertical displacement response of the observation point. The results are in a good agreement. At the beginning, all three methods show excellent agreement between results. Differences start to occur after the peak displacement is reached. The BEM produces larger peak than the SBFEM and EMM, while for the late times the BEM solution approaches SBFEM solution.

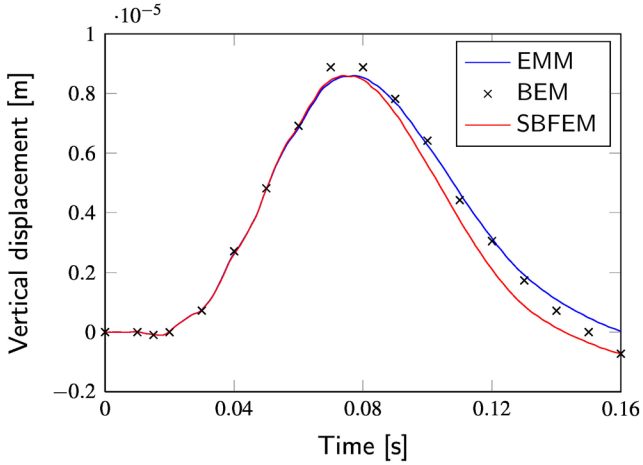

Figure 10. Comparison of the vertical displacement response of the observation point computed using three different methods to model unbounded soil – BEM, EMM and SBFEM.

3.2 Rigid massless disk foundation resting on the surface of a half-space

The following example compares the accuracy of the SBFE, extended mesh (EMM) and lumped-parameter methods.

The structure is a rigid massless disk resting on the surface of the elastic undamped homogenous isotropic half-space. The radius of the disk is denoted r. The half-space has a shear modulus G_s, mass density ρ, shear wave velocity $c_s = \sqrt{(G_s/\rho)}$ and Poisson's ratio $\upsilon = 0.3$.

Lumped-parameter model 1 (Figure 11a) comprises one static stiffness parameter K_0 (chosen to match the static stiffness of the site) and four dynamic parameters – two masses M_0 and M_1, and two dashpots C_0 and C_1 (Equation 13) – obtained through curve fitting to the dynamic stiffness of the site[3].

$$C_{0,1} = (r/c_s)K_0\gamma_{0,1} \quad , \quad M_{0,1} = (r/c_s)^2 K_0\mu_{0,1} \qquad (13)$$

This model of the half-space is doubly asymptotic – it represents the dynamic stiffness of the half-space exactly at the static ($f \to 0$) and at the high-frequency limit ($f \to \infty$). In between these limits, lumped-parameter model 1 represents the dynamic stiffness only approximately. The dimensionless coefficients of model 1 are given in Table 1.

Lumped parameter model 2 (Figure 11b) is based on the propagation of waves in the semi-infinite truncated cones [4][16]. Similar to lumped-parameter model 1, this model is based on the combination of frequency independent spring, mass and dashpot elements. This model is also doubly asymptotic. Discrete coefficients are given in Table 2 (with $A = \pi r^2$ and $I = \pi r^4/4$).

For the EMM, a significantly large portion of the half-space is modelled with eight-node brick finite elements so that the waves which are reflected from the boundary do not return back before the end of the observation time. As shown in Figure 11c (blue), a cylindrical mesh with the radius and height $10r$ is used to model the extended mesh. The rigid disk (red) is modelled with four-node quadrilaterals.

The SBFEM model is shown in Figure 11d. As for EMM, the circular foundation on the surface is modelled with four-node quadrilaterals (purple), and the material properties are chosen such that it can be regarded as rigid ($E_f/E_s > 10^4$). In order to apply the scaled boundary finite-elements, the soil-structure interface must be discretized with at least one row of elements embedded in the half-space and must be entirely visible from the chosen scaling point (centre of the disk). Since the disk is resting on the half-space surface, the soil-structure interface must be moved slightly away from the foundation in order to apply the scaled boundary finite-elements. This is achieved by four rows of eight-node brick elements which are used to model soil in the immediate vicinity of the disk (soil near-field). Scaled boundary finite elements are then applied at the interface between brick elements and the surrounding soil (Figure 11d, yellow quads). The mesh for the EMM model is finer than the mesh for the SBFEM model in the radial direction.

The acceleration unit-impulse response matrix is calculated using the new procedure proposed in this paper, with integration parameters $M = 10$, $N = 5$ and $\theta = 1.4$.

Vertical, horizontal and rocking response due to the corresponding triangular impulse load is calculated using a time step size $\Delta t = 0.05b/c_s$. The results are shown in Figures 12a-c.

The SBFEM procedure shows excellent agreement with the EMM method. Because they comprise frequency independent spring, dashpot and mass elements, lumped-

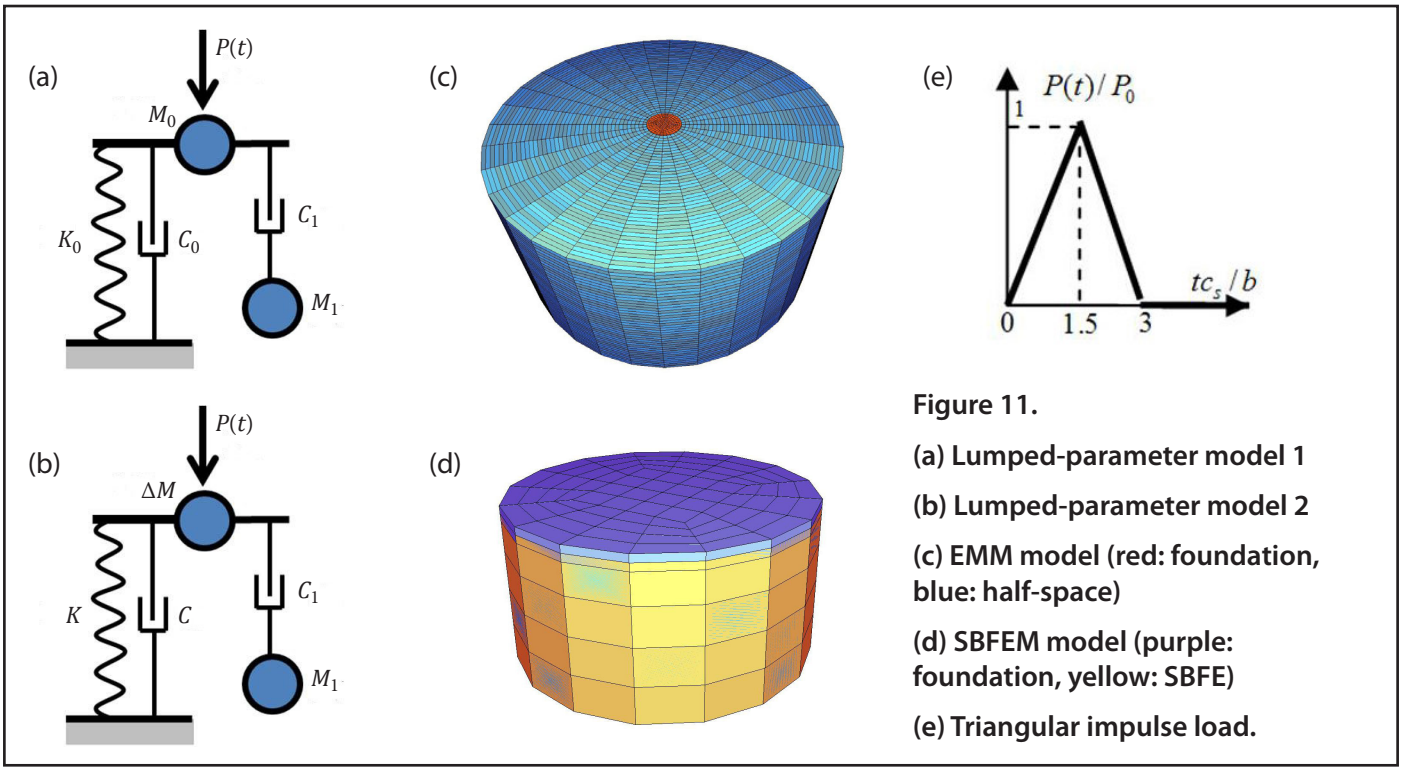

Figure 11.

(a) Lumped-parameter model 1

(b) Lumped-parameter model 2

(c) EMM model (red: foundation, blue: half-space)

(d) SBFEM model (purple: foundation, yellow: SBFE)

(e) Triangular impulse load.

dof	u_V	u_H	φ
K_0	$\frac{4G_s r}{1-\nu}$	$\frac{8G_s r}{2-\nu}$	$\frac{8G_s r^3}{3(1-\nu)}$
γ_0	0.8	$0.78-0.4\nu$	-
γ_1	$0.34-4.3\nu^4$	-	$0.42-0.3\nu^2$
$\mu_0 \geq 0$	$0.9(\nu-1/3)$	-	$0.16(\nu-1/3)$
μ_1	$0.4-4\nu^4$	-	$0.34-0.2\nu^2$

Table 1. Dimensionless coefficients of lumped-parameter model for vertical motion of a disk foundation.

dof	u_V	u_H	φ
	$K=\rho c^2 A/z_0$ $C=\rho cA$		$K=3\rho c^2 I/z_0$ $C_1=\rho cI$ $M_1=\rho I z_0$
ΔM	0 $2.4(\nu-1/3)\rho A r$	-	0 $1.2(\nu-1/3)\rho I r$
c	c_p $2c_s$	c_s	c_p $2c_s$
$\frac{z_0}{r}$	$\frac{\pi}{8}(1-\nu)\left(\frac{c}{c_s}\right)^2$	$\frac{\pi}{8}(1-\nu)$	$\frac{9\pi}{32}(1-\nu)\left(\frac{c}{c_s}\right)^2$

Table 2. Coefficients of lumped-parameter model 2. For wave velocity c and trapped mass ΔM upper values are valid for $\nu \leq 1/3$ and lower for $1/3 < \nu \leq 1/2$.

parameter models can only approximately model dynamic stiffness. The accuracy of the approximation depends on the frequency range. For this relatively simple example of a rigid disk on a homogeneous half-space, both lumped-parameter models behave well and show only small deviation from the results obtained by EMM and SBFEM methods. However, for more complicated practical examples (flexible foundations, non-homogeneous soil) the approximation of the dynamic stiffness inherent in lumped parameter models can often be too crude to be used for modelling of the dynamic soil-structure interaction effects.

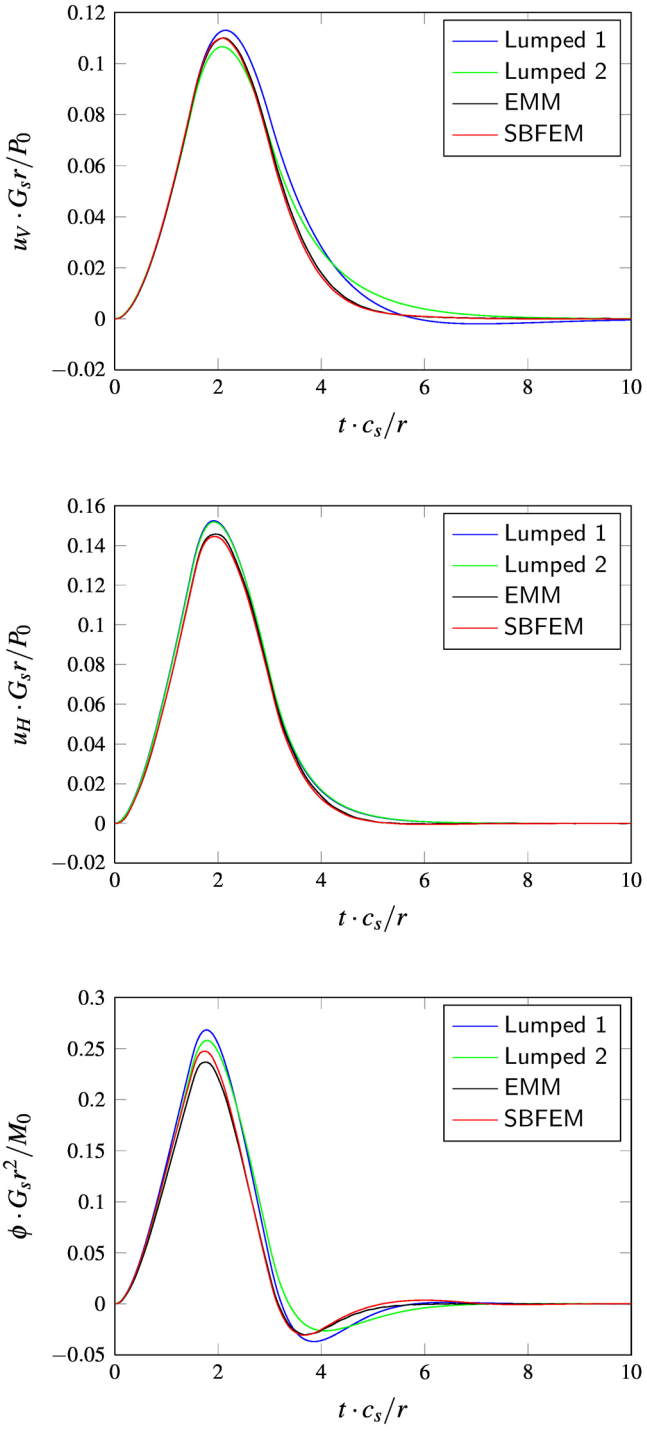

Figure 12. Vertical, horizontal and rocking response of the rigid massless disk foundation.

3.3 Water tank subjected to seismic excitation

A reinforced concrete water tank is considered in seismic analysis (Figure 13). One quarter of the model of the tank is shown in Figure 13. In reality, a full three-dimensional example is analysed.

The cylindrically shaped concrete tank (orange) has a radius r_t = 44.3m, height h_t = 34.25m (level t) and thickness t_t = 0.6m. The roof of the tank is spherically shaped with a radius r_r = 85m, thickness t_r = 0.3m and a central point at the height h_r = 46.71m (level r) from the ground. The foundation plate (yellow) is a circular disk resting on a surface of the soil (level f) with a radius r_f = 45.8m and a thickness t_f = 0.5m. The material for both the tank and the foundation plate is concrete of EC class 40. Four-node quadrilateral finite elements are used for the modelling of the tank and the foundation plate. Stiffness and mass proportional Rayleigh damping is assigned to the tank with a 3% viscous damping ratio at frequencies 0.25Hz and 20Hz.

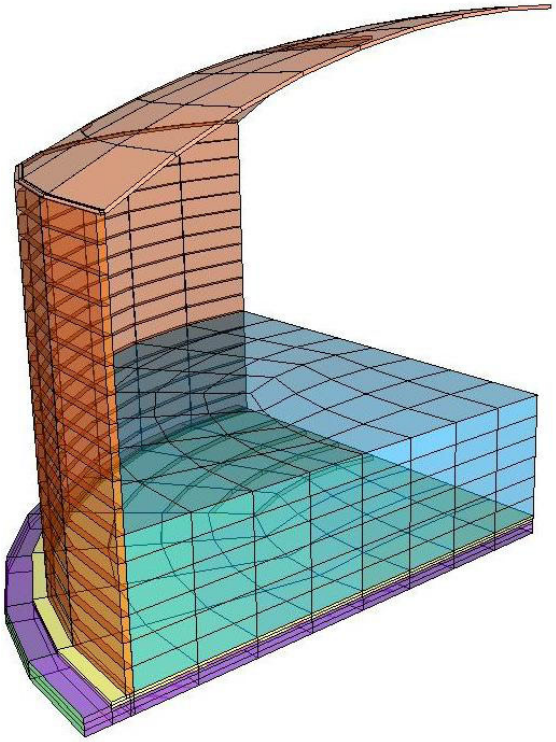

Figure 13. Quarter of the FEM-SBFEM model of the water tank (orange: tank, blue: water, yellow: foundation plate, purple: soil near-field, green: soil far-field).

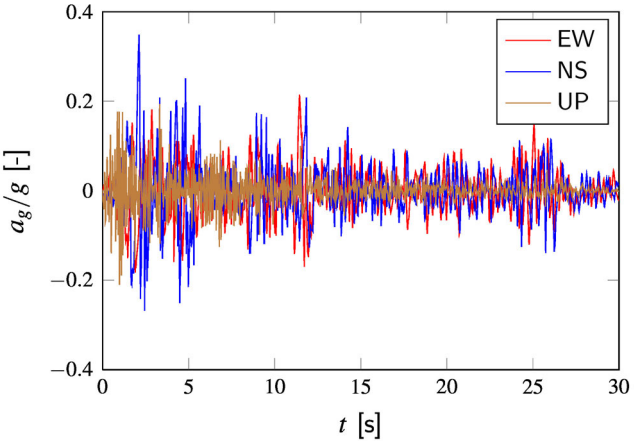

Figure 14. Three components of the El-Centro earthquake: East-West (x-axis, $\max|a_{gx}| = 0.21$g), North-South (y-axis, $\max|a_{gy}| = 0.35$g) and Up (z-axis, $\max|a_{gz}| = 0.21$g).

Three-dimensional Lagrangian fluid finite elements (blue) have been utilized in order to model the water inside the tank. Very small shear modulus and a Poisson's ratio of nearly 0.5 have been assigned to the eight-node volume fluid finite-elements. The tank is filled with water up to the level of 12.25m above the ground (level w).

The soil is modelled as a homogeneous, linear-elastic half-space without material damping. The mass density of the soil is $\rho_s = 2.0\text{t/m}^3$ while Poisson's ratio is $\nu_s = 0.3$. Shear wave velocity of the soil c_s is varied between the lowest value of 100m/s (soft soil) and the highest of 1000m/s (rock). The near-field soil (purple) consists of three layers of eight-node volume finite elements down to a depth of 1.5m. Scaled boundary four-node quadrilateral finite elements (green) are used for modelling the far-field soil stretching to infinity. These elements are applied at the immediate boundary between the near- and the far-field (Figure 13). The scaling point coincides with the origin of the coordinate system (centre of the foundation plate).

In the seismic analysis the tank is subjected to three components of motion of the El-Centro earthquake (Figure 14). Seismic excitation in form of a ground acceleration vector $\ddot{\mathbf{u}}^g(t)$ (Equation 1) is applied at the soil-structure interface nodes (scaled boundary finite element nodes). Since the SSI-interface is close to the surface of the soil (half-space) we assume that the scattered and the free-field motion are the same. In this example all the SSI-interface nodes are excited with the same ground acceleration (synchronous oscillation without phase shift). In reality due to the large diameter of the structure, the spatial variation of the seismic wave field should be taken into consideration.

Integration of the governing dynamic equations of motion of the water tank-soil system (Equations 1 and 2) has been performed for the total of $n = 1500$ time steps of the size $\Delta t = 0.02$s resulting in the total time of $t_{\max} = 30$s. Parameters for the determination of the acceleration unit-impulse response matrix using a new procedure are $M = 10$, $N = 5$ and $\theta = 1.4$.

Absolute peak accelerations in the x-direction along the height of the XZ cross section of the tank are shown in Figure 15. Similarly, Figure 16 shows the y-component absolute peak accelerations in the YZ cross section of the tank. Values are normalized with respect to the gravity acceleration g. The four levels of most interest are the foundation plate (f), water surface (w), top of the tank (t) and the top of the roof level (r).

The presence of the water alters the response of the tank in a way that the local maximum of the absolute peak accelerations of the tank appears approximately at the water level (w), independently of the properties of the soil. Other local maxima occur at the top of the tank (t) and the top of the roof level (r). Minimum absolute peak acceleration is always at the ground level (foundation plate level), and it is almost the same as the peak acceleration of the prescribed El-Centro earthquake excitation (Figure 14). These extreme values appear within the first 5 seconds of the earthquake.

Time histories of the x-component of the acceleration for four levels of the XZ cross section of the tank are plotted on Figure 17. The shear wave velocity of the soil is kept fixed at 250m/s. Only the first 10 of the total 30 seconds of analysed time are shown.

Time histories of the y-component of the acceleration at

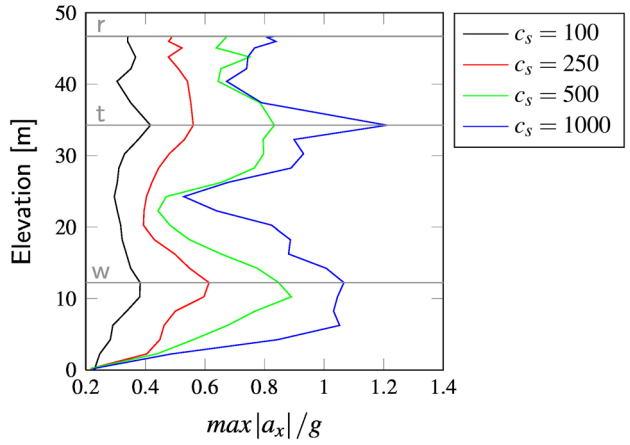

Figure 15. Absolute peak x-component acceleration along the height of the XZ cross section of the tank.

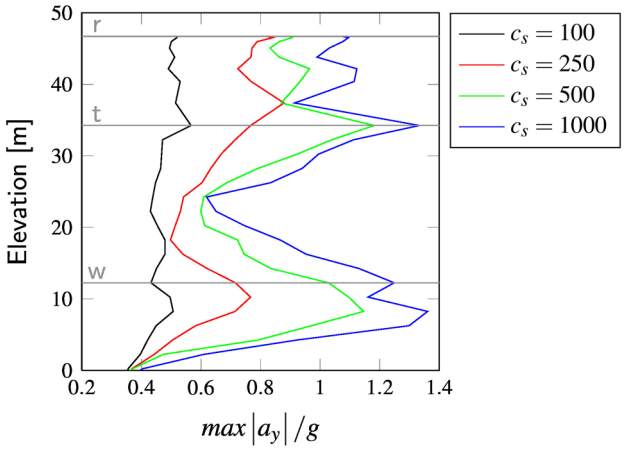

Figure 16. Absolute peak y-component acceleration along the height of the YZ cross section of the tank.

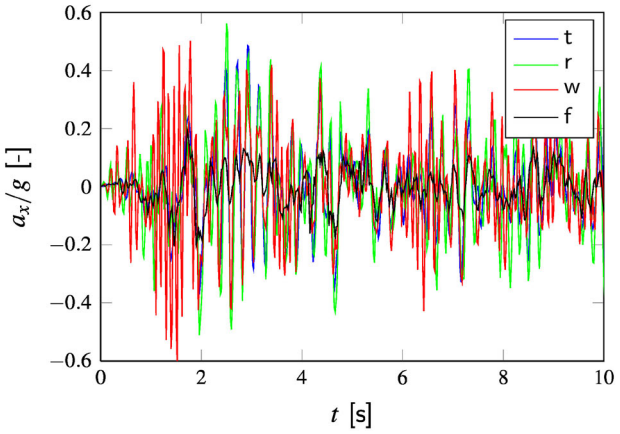

Figure 17. X-component of the acceleration time history of the foundation (f), water surface (w), top of the tank (r) and the top of the roof (t) level of the XZ cross section of the tank for $c_s = 250\text{m/s}$.

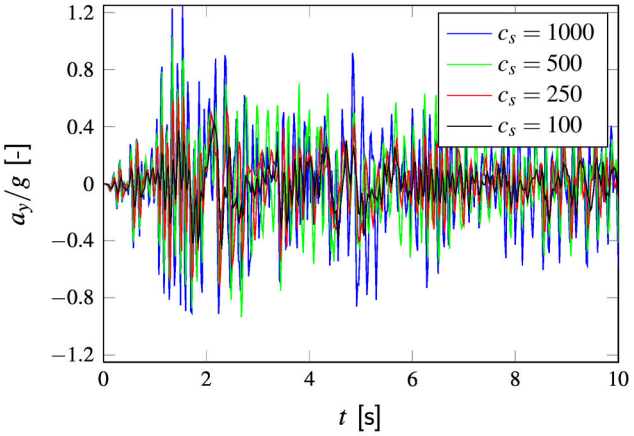

Figure 18. Y-component acceleration time history at the water surface level (w) of the YZ cross section of the tank.

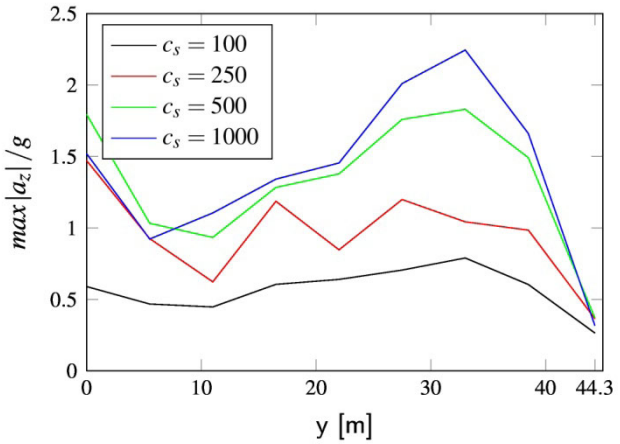

Figure 19. Vertical component of the absolute peak acceleration of the roof of the tank for the points along the y-axis ($y = 0$ – centre of the roof, $y = 44.3\text{m}$ – tank wall)

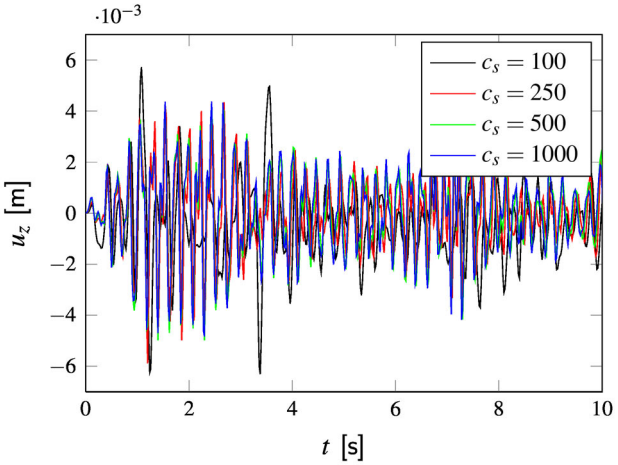

Figure 20. Vertical displacement time history of the top of the roof of the tank.

the water surface level of the *YZ* cross section of the tank are depicted on Figure 18.

Figure 19 shows the absolute peak vertical acceleration of the roof of the tank for the points along the *y*-axis, depending on the properties of the soil. Interestingly, the maximum absolute peak acceleration, except for the case $c_s = 250$m/s, does not appear at the centre of the roof, but at the distance of approximately 10m from the tank wall. This is due to the fact that the dominant vertical vibration mode of the roof is an asymmetric one.

How pronounced the SSI effects will be depends on the ratio of the stiffness of the structure to the stiffness of the soil. As this ratio grows, so does the effect that the soil has on the dynamic behaviour of the soil-structure system. This is evident from Figures 15-19. For this example the soil-structure interaction in general plays a beneficial role in a sense that it reduces the maximum accelerations of the tank compared to the fixed-base solution (structure founded on a stiff rock). Maximum amplification ratio for the accelerations in *y*-direction (ratio of the maximal acceleration of the structure to the maximal ground acceleration) for the soft soil (1.6) is reduced by a factor of 2 compared to the solution founded on a hard rock (3.4) (Figure 16). Things are even more dramatic for the *x*- and *z*-direction where this factor grows to 3 (Figures 15 and 19).

The same cannot be said for the displacements. Figure 20 shows the vertical displacement response history of the top of the roof depending on the stiffness of the soil. Although less sensitive to the changes of the properties of the soil than the accelerations, it can be observed that the displacements grow inversely proportional to the ratio of the stiffness of the structure and the soil.

4 Conclusion

A new procedure for the treatment of the three-dimensional dynamic analysis of soil-structure interaction in time domain, where the soil is modelled using the scaled boundary finite-element method (SBFEM) is described. Two essential improvements are employed to the original method which is based on the piece-wise constant approximation of the acceleration unit-impulse response matrix and evaluation of time-consuming convolution integrals: (1) The acceleration unit-impulse response matrix of the unbounded soil is determined using a new integration scheme based on the piece-wise linear approximation within one time step and an extrapolation parameter which increases stability of the scheme and allows the use of the larger time steps. The efficiency of the scheme is increased even further by employing the truncation time after which the acceleration unit-impulse response matrix is linearized. Unlike other approximations that employ the truncation of the solution of the acceleration unit-impulse response matrix as well, the new procedure is robust and it allows the error introduced by the truncation to be controlled by the prescribed error tolerance. (2) The soil-structure interaction force vector represented by the convolution integral is evaluated using a new and very efficient scheme based on the integration by parts. This scheme also allows only a portion of the entire time history of the displacement and velocity vectors to be kept in memory, and a cyclic buffer can be used in order to reduce memory storage. The combination of the two aforementioned enhancements leads to a very significant reduction of computational effort and linear dependency with respect to the number of time steps after the truncation time.

In the second part of the paper, two- and three-dimensional benchmark and practical examples of the dynamic soil-structure interaction are analysed. The results obtained by the scaled boundary finite element procedure are compared with the commonly used procedures like the lumped-parameter or the boundary element method. These examples demonstrate the accuracy and computational efficiency of the proposed method, qualifying the new approach for the usage in large practical problems encountered in vibration and earthquake engineering.

References

[1] Mylonakis G, Syngros C, Gazetas G & Tazo T (2006). The role of soil in the collapse of 18 piers of Hanshin Expressway in the Kobe earthquake. *Earthquake Engineering and Structural Dynamics*, **35**, 547-575.

[2] Wolf JP (1985). *Dynamic Soil-Structure-Interaction Analysis*. Prentice-Hall, Englewood Cliffs, NJ.

[3] Wolf JP (1988) *Soil-Structure-Interaction Analysis in Time Domain*. Prentice-Hall, Englewood Cliffs, NJ.

[4] Wolf JP (1994). *Foundation Vibration Analysis Using Simple Physical Models*. Prentice-Hall, Englewood Cliffs, NJ.

[5] Wolf JP & Song C (1996). *Finite-Element Modelling of Unbounded Media*. John Wiley and Sons, Chichester, UK.

[6] Wolf JP (2003). *The Scaled Boundary Finite Element Method*. John Wiley and Sons, Chichester, UK.

[7] Bazyar MH & Song C (2006). Time-harmonic response of non-homogeneous elastic unbounded domains using the scaled boundary finite-element method. *Earthquake Engineering and Structural Dynamics*, **35**, 357-383.

[8] Bazyar MH & Song C (2006). Transient analysis of wave propagation in non-homogeneous elastic unbounded domains by using the scaled boundary-finite element method. *Earthquake Engineering and Structural Dynamics*, **35**, 1787-1806.

[9] Radmanović B & Katz C (2010). A High Performance Scaled Boundary Finite Element Method. *IOP Conference Series: Materials Science and Engineering*, **10**, 012214.

[10] Radmanović B & Katz C (2011). Dynamic Soil-

Structure Interaction Using a High Performance Scaled Boundary Finite Element Method in Time Domain. *Proceedings of the 8th International Conference on Structural Dynamics*, EURODYN 2011, Leuven, Belgium, 4-6 July 2011, 503-510.

[11] Zhang X, Wegner JL & Haddow JB (1999). Three-dimensional dynamic soil-structure interaction analysis in the time domain. *Earthquake Engineering and Structural Dynamics*, **28**, 1501-1524.

[12] Yan J, Zhang C & Jin F (2004). A coupling procedure of FE and SBFE for soil-structure interaction in the time domain. *International Journal for Numerical Methods in Engineering*, **59**, 1453-1471.

[13] Lehmann L (2005). An effective finite element approach for soil-structure analysis in the time domain. *Structural Engineering and Mechanics*, **21**, 437-450.

[14] Lehmann L (2007). *Wave Propagation in Infinite Domains: With Applications to Structure Interaction*. Springer, Berlin, Germany.

[15] Stamos AA, Estorff OV, Antes H & Beskos DE (1994). Vibration Isolation in road-tunnel traffic systems. *International Journal for Engineering and Design*, **1**, 109-201.

[16] Wolf JP & Deeks AJ (2004). *Dynamic Soil-Structure-Interaction Analysis*. Prentice-Hall, Englewood Cliffs, NJ.

Notable Earthquakes July – October 2011

Reported by British Geological Survey

Issued by: Davie Galloway, British Geological Survey, January 2012.
Non British Earthquake Data supplied by The United States Geological Survey.

Year	Day	Mon	Time UTC	Lat	Lon	Dep km	Magnitude M_L	Magnitude M_b	Magnitude M_W	Location
2011	06	JUL	19:03	29.54S	176.34W	17			7.6	KERMADEC ISLANDS
2011	10	JUL	00:57	38.03N	143.26E	23			7.0	HONSHU, JAPAN
2011	14	JUL	06:59	50.12N	0.74W	10	3.9			ENGLISH CHANNEL
Felt in southern coastal towns from Portsmouth to Eastbourne (3 EMS).										
2011	14	JUL	13:30	50.11N	0.73W	10	1.8			ENGLISH CHANNEL
2011	14	JUL	20:55	50.08N	0.60W	10	1.8			ENGLISH CHANNEL
2011	19	JUL	19:35	40.08N	71.41E	20			6.1	KYRGYZSTAN
At least 13 people killed, 86 others injured and several buildings destroyed in Farg'ona, Uzbekistan and one other person killed in Khujand, Tajikistan.										
2011	21	JUL	14:21	53.58N	2.24E	12	3.5			SOUTHERN NORTH SEA
2011	29	JUL	07:42	23.78S	179.76E	523			6.7	FIJI ISLANDS REGION
2011	30	JUL	15:56	57.03S	5.51W	10	1.7			KNOYDART, HIGHLAND
2011	31	JUL	23:58	3.52S	144.83E	10			6.6	PAPUA NEW GUINEA
2011	04	AUG	16:45	52.25N	2.84W	8	2.0			LEOMINSTER, HEREFORD
2011	04	AUG	23:25	54.58N	1.99W	2	2.0			BARNARD CASTLE, DURHAM
2011	11	AUG	10:06	39.96N	77.03E	10			5.6	SOUTHERN XINJIANG
Twenty people injured and moderated damage reported in Kashi.										
2011	20	AUG	16:55	18.36S	168.14E	32			7.2	VANUATU
2011	20	AUG	18:19	18.31S	168.22E	28			7.1	VANUATU
2011	21	AUG	08:37	56.85N	5.67W	12	2.9			LOCHAILORT, HIGHLAND
Felt Lochailort, Glenfinnan and Acharacle (3 EMS).										
2011	21	AUG	18:24	56.87N	5.67W	11	2.0			LOCHAILORT, HIGHLAND
Felt Lochailort and Acharacle (3 EMS).										
2011	23	AUG	17:51	37.94N	77.93W	6			5.8	VIRGINIA, USA
Damage reported from the epicentral area. Washington National Cathedral was damaged and the Washington Monument closed.										

Year	Day	Mon	Time UTC	Lat	Lon	Dep km	Magnitude M_L	Magnitude M_b	Magnitude M_W	Location
2011	24	AUG	17:46	7.64S	74.53W	147			7.0	NORTHERN PERU
2011	29	AUG	10:08	56.70N	5.20W	7	1.9			BALLACHULISH, HIGHLAND
Felt Ballachulish, Glencoe, Appin and Fort William (3 EMS).										
2011	02	SEP	10:55	52.17N	171.71W	32			6.9	ALEUTIAN ISLANDS
Tsunami with a wave height of 6cm was recorded on Atka Island.										
2011	02	SEP	13:47	28.40S	63.03W	579			6.7	ARGENTINA
2011	03	SEP	22:55	20.67S	169.72E	185			7.0	VANUATU
2011	05	SEP	02:23	51.99S	1.80E	11	1.8			SOUTHERN NORTH SEA
2011	05	SEP	17:55	2.97N	97.89E	91			6.7	NORTHERN SUMATRA
At least 10 people killed in Aceh.										
2011	08	SEP	10:41	56.59N	5.64W	6	1.9			LOCHALINE, HIGHLAND
2011	08	SEP	19:02	51.79N	5.84E	10	4.5			THE NETHERLANDS
Felt The Netherlands, Germany and Belgium (5 EMS).										
2011	14	SEP	17:56	56.34N	5.12W	12	2.1			INVERARAY, ARGYLL/BUTE
2011	15	SEP	19:31	21.61S	179.53W	645			7.3	FIJI ISLANDS REGION
2011	16	SEP	19:26	40.27N	142.78E	33			6.7	HONSHU, JAPAN
2011	18	SEP	12:40	27.72N	88.14E	50			6.9	SIKKIM, INDIA
At least 94 people killed, hundreds injured and several thousand buildings and many bridges and roads damaged in the Sikkim/West Bengal area. Six people killed, 25 more injured and over 4,000 buildings damaged in Bhojpur, Ilam and Panchthar, Nepal. Seven people killed and 136 injured in Tibet, China and a further person killed and 16 others injured in Paro-Thimphu region, Bhutan. The total economic loss in India is estimated at $US 22.3 billion.										
2011	19	SEP	18:33	14.19N	90.24W	9			5.6	GUATEMALA
One person killed in Guatemala.										
2011	03	OCT	21:12	56.23N	3.58W	8	1.6			GLENDEVON, PERTHSHIRE
Felt Glendevon and Carnbo (3 EMS).										
2011	04	OCT	08:15	56.23N	3.58W	9	1.4			GLENDEVON, PERTHSHIRE
Felt Glendevon (2 EMS).										
2011	09	OCT	04:33	53.27N	4.09E	10	2.7			SOUTHERN NORTH SEA
2011	12	OCT	06:37	65.90N	0.24E	15	3.0			NORWEGIAN SEA
2011	13	OCT	03:16	9.34S	114.59E	3			6.1	BALI, INDONESIA
At least 43 people injured in southern Bali.										
2011	14	OCT	03:35	6.57S	147.88E	37			6.5	EASTERN NEW GUINEA
2011	19	OCT	02:32	53.21N	0.89W	1	1.6			OLLERTON, NOTTS
Felt New Ollerton (3 EMS).										
2011	20	OCT	16:52	57.16N	5.48W	14	2.4			GLEN SHEIL, HIGHLAND
2011	21	OCT	09:11	62.00N	2.27E	10	3.5			NORTHERN NORTH SEA
2011	21	OCT	17:57	29.04S	176.22W	33			7.4	KERMADEC ISLANDS
2011	23	OCT	10:41	38.69N	43.50E	16			7.1	EASTERN TURKEY
Over 600 people killed, some 2,500 others injured, at least 10,600 buildings either destroyed or damaged and telecommunications, electricity and water services disrupted in the Ercis/Tabanli/Van areas.										
2011	28	OCT	18:54	14.44S	75.97W	24			6.9	COAST OF CENTRAL PERU
One person killed in San Vicente de Canete and over 100 people injured and 134 buildings destroyed in Ica.										
2011	31	OCT	23:26	56.51N	4.32W	3	1.8			KILLIN, STIRLING
Felt Killin, Stirling) and Aberfeldy, Perth and Kinross (3 EMS).										

Letters

In response to the article on EEFIT in the last Newsletter by Edmund Booth *et al*., Roy Severn has sent the following comment.

EEFIT – The beginning

In the late 1970s I was a member of the SRC Engineering Board, which had a Civil Engineering Sub-committee whose Chairman was Leslie Sallabank, a Contractor involved in nuclear power station construction, but very aware of the immediate need to increase research in civil engineering. Sometime in this period the SRC found that its budget for that financial year would be underspent, allowing it to commit the underspend to capital projects, to be committed before the end of the financial year. Leslie Sallabank seized on this, obtaining c. £4 million for civil engineering research infrastructures.

Small groups, including some from the industry, were established to decide on appropriate sites, resulting in decisions to create a new flume at Wallingford, a soil mechanics research site at Bothkennar in Scotland, an anaerobic treatment plant based at Birmingham University, and a 6DOF shaking table at Bristol University. In association with the last of these was a recommendation that, in view of there not being much experience of major earthquakes in the UK, the SRC should commit a small budget for providing expenses of university researchers to visit sites where major earthquakes had occurred. Leslie Sallabank undertook to persuade industry to similarly fund its young engineers, and I was made responsible for getting it off the ground and coordinating its visits. Thus was EEFIT born!

It was clearly a success, ensuring that, in due course, both SERC and now EPSRC have continued the funding, as have the profession.

Forthcoming events

Date	Venue	Title	People
27/03/2012 at 17:45	University of Manchester Renold Building	*Seismic design of bridges*	*Speaker*: **Thanos Bistolas** (Mott MacDonald) Organised by ICE Manchester Branch in conjunction with IStructE
28/03/2012 at 18:00	Imperial College London South Kensington Campus Skempton Building	*Adding damping in flexible structures*	*Speaker*: **Daniel Powell** (Arup) *Organiser*: **Damian Grant** (SECED / Arup)
28-30/05/2012	Taormina (Italy)	*Second International Conference on Performance-Based Design in Earthquake Geotechnical Engineering*	Organised by the Italian Geotechnical Association

For up-to-date details of SECED events, visit the website: **www.seced.org.uk**

SECED Newsletter

The SECED Newsletter is published quarterly. All contributions of relevance to the members of the Society are welcome. Manuscripts should be sent by email. Diagrams, pictures and text should be attached in separate electronic files. Hand-drawn diagrams should be scanned in high resolution so as to be suitable for digital reproduction. Photographs should likewise be submitted in high resolution. Colour images are welcome. Hard copy manuscripts are also welcome. Please contact the Editor of the Newsletter, Andreas Nielsen, for further details: email: andreas.nielsen@jacobs.com; telephone: 0141 243 8418.